Butterfly Mesogens Based on Carbazole, Fluorene or Fluorenone: Mesomorphous, Gelling, Photophysical, and Photoconductive Properties

Jun-fang Hang, Hang Lin, Ke-qing Zhao, Ping Hu, Bi-qin Wang, Hirosato Monobe, Chenhui Zhu, Bertrand Donnio

Butterfly Mesogens Based on Carbazole, Fluorene or Fluorenone: Mesomorphous, Gelling, Photophysical, and Photoconductive Properties

Jun-Fang Hang,[a] Hang Lin,[a] Ke-Qing Zhao,*[a] Ping Hu,[a] Bi-Qin Wang,[a] Hirosato Monobe,*[b] Chenhui Zhu,[c] and Bertrand Donnio*[d]

Cite as *Eur. J. Org. Chem.* 2021, *16*, 1106-1117
Publication Date: February 26, 2021
https://doi.org/10.1002/ejoc.202100108

A generic synthetic method based on the Suzuki-Scholl reactions was successfully exploited to yield new poly(hetero)aromatic hydrocarbons containing carbazole, fluorene or fluorenone moieties. These butterfly-like mesogens exhibit columnar mesophases, form fibrous gels in various solvents, emit blue to orange light in films and solutions and show outstanding photocurrent behavior with charge carrier mobility in the ~0.03 $cm^2 V^{-1} s^{-1}$ range.

Abstract: We report a straightforward and generic synthesis of several new series of annulated π-extended poly-(hetero)aromatic hydrocarbons (PAH), with carbazole, fluorene and fluorenone central building blocks by the Suzuki-Miyaura/Scholl tandem reactions. The corresponding series of ditriphenylene discogens with a carbazole or a fluorenone central core, respectively, possess hexagonal columnar mesophases with broad mesophase ranges and high clearing points, as well as demonstrate a strong aggregation tendency in organic solvents as supergelators. The laterally-substituted ditriphenylene mesogens based on dimethyl-fluorene core exhibit a rich polymorphism with rectangular and hexagonal columnar mesophases from low temperatures onward, whereas their dioctyl-fluorene homologues melt directly into the isotropic liquid without showing mesophases. These latter family of compounds are luminescent with very high fluorescent quantum yields, of around 70 % in solution, and show outstanding photocurrent behavior with charge carrier mobility in the 10^{-2} $cm^2 V^{-1} s^{-1}$ range, as measured by photocurrent transient time-of-flight (TOF) technique. This straightforward molecular design and simple synthetic strategy proved to be both potent and resilient, and could be generally applied to the fabrication of a great variety of other heteroarene molecular systems as organic semiconductors and electroluminescent materials for potentially low-cost applications.

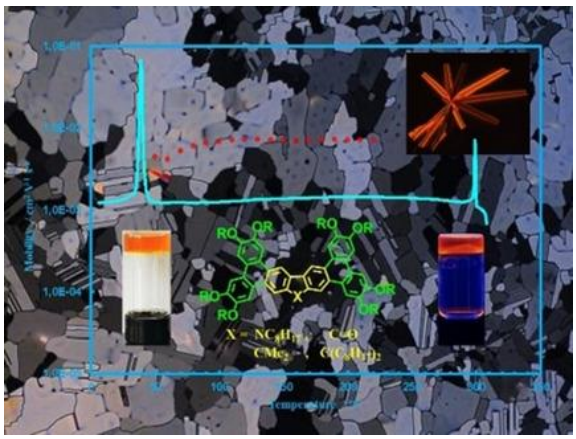

Introduction

Conjugated polymers with carbazole, fluorene and fluorenone building blocks are important plastic electronic materials and widely studied as active layers for various electronic devices, such as organic light-emitting diodes (OLED),[1] organic photovoltaic cells (OPV)[2] and organic field-effect transistors (OFET).[3] The corresponding low-molecular weight liquid crystalline systems and oligomers based on these three building blocks also exhibit outstanding optical/electronic properties in addition to show spontaneous self-organization behavior. They have however been much less investigated than their polymeric counterparts due essentially to some chemical/thermal/photo stability, solubility or processability issues.

Particularly promising, π-conjugated polyfused (hetero)aromatic hydrocarbons (PAH) forming discotic liquid crystals (DLCs) are considered to play a crucial role in the next generation of organic semiconductors. They can indeed exhibit one-dimensional high charge carrier (electrons or holes) mobility values due to their propensity to self-organize into long-range ordered supramolecular columns,[4] and their unique structural defects self-healing capability, chemical robustness and cost-effective solution-processed electronic devices fabrication represent interesting and competitive assets in the field of organic semiconductors.

Carbazole-containing liquid crystals with nematic (N) and smectic A (SmA) phases have been applied in OLED for hole transport layers[5] or light-emitting layers,[6] while their mesophase types, transition temperatures and solubility could be modulated by the alkyl chain length grafted onto the N-atom. However, the molecular engineering of carbazole derivatives for columnar mesophase did not initially succeed. First successful attempts combining triphenylene and carbazole units, connected through flexible spacers into dyads and heptamers were only recently reported.[7] Recent molecular designing strategies using carbazole as the discotic core[8] or directly sigma-bonded triphenylene-carbazole,[9] star-shaped triazine-carbazole[10] were successful in the construction of columnar mesophase materials as electronic conductors. Other ordered electronic materials such as co-dendrimers made of carbazole/mesogen mixtures[11] were also reported to possess mesomorphous behavior and good electronic properties.

Structurally similar to carbazole, π-conjugated fluorene rigid building block is also capable of yielding potentially interesting opto-electronic mesogenic materials. Fluorene rod-like liquid crystals were reported to exhibit N and SmA phases, and fabricated for polarizing OLED.[12] Further, deep-blue emissive spiro-fluorene derivatives[13] were tuned to displaying columnar rectangular/hexagonal mesophases. Wong studied star-shaped hexabenzocoronene-fluorene systems[14] as discotic columnar electronic materials and investigated their performance in OPV and OFET devices.[15] Triphenylene-fluorene dyads and triads, showing nematic and hexagonal columnar mesophases with high charge carrier mobility were also recently reported.[16]

Similarly, fluorenone is another attractive building block, as its planar structure and functional polar ketone group are beneficial for promoting closer π-π stacking and monitoring optical/electronic properties modulation. Some mesogenic fluorenones with SmA phase exhibited hole mobility of 10^{-2} $cm^2\ V^{-1}\ s^{-1}$,[17] and power conversion efficiency of 0.8 % in solar cells.[18] Until now, not many examples of π-extended mesogenic electronic materials inserting carbazole, fluorene and fluorenone building blocks, such as in triindoles,[19] truxenes[20] and truxenones,[21] have been reported, despite their great potential for the further development of organic electronic materials-based devices.

In this work, we report the general synthesis of three novel families of butterfly-like molecules based on ditriphenylenes fused with carbazole, fluorene and fluorenone central cores, respectively (Figure

1). Starting from the commercially available carbazole, fluorene and fluorenone building blocks, the three series of annulated ditriphenylene compounds were obtained by the combination of two emblematic chemical reactions, namely the $Pd(PPh_3)_4$-catalyzed Suzuki-Miyaura cross-coupling[22] and the $FeCl_3$-catalyzed Scholl[23] intramolecular oxidative cyclo-dehydrogenation. Their liquid crystalline and gel self-assemblies were investigated, and their optical and charge carrier properties were evaluated.

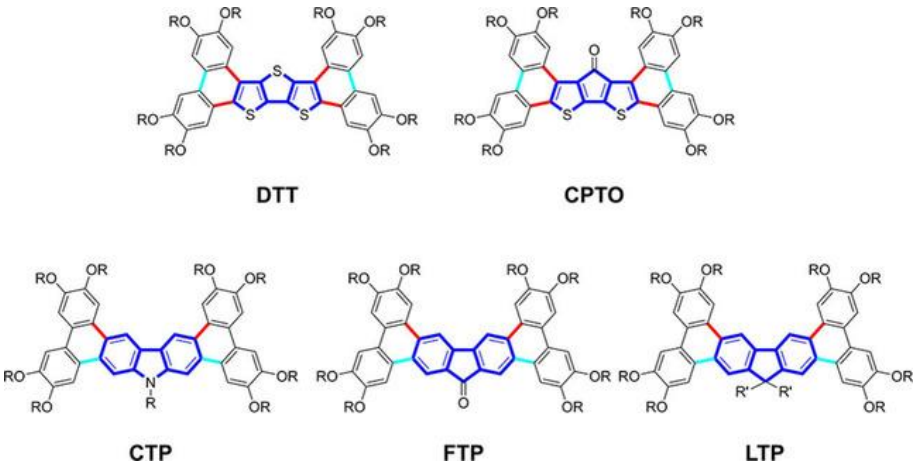

Figure 1. Examples of some previously and currently reported butterfly-like mesomorphous heteroarenes containing tristhiophene (**DTT**),[24] cyclopentan-dithiophen-4-one (**CPTO**),[25] carbazole (**CTP**), fluorenone (**FTP**) and fluorene (**LTP**) building blocks, respectively.

Results and Discussion

Rational molecular design and synthesis Planar, polycyclic aromatic hydrocarbons (PAH) with multiple peripheral alkyl chains are typical discotic liquid crystals (DLCs) and can be considered as potential organic one-dimensional semiconductors due to their high propensity to self-organize into supramolecular columns and to favor the unidirectional mobility of the charges (electrons or holes). Flexibility and rigidity of the molecular conformation as well as the number and length of the irradiating aliphatic chains have been used to modulate supramolecular packing and liquid crystalline properties. Despite active research in the field of molecular electronic, the diversity of charge carrying DLCs remains however quite limited, though it is increasing steadily with the progress and implementation of original synthetic strategies and with the increasing availability of some key functional building blocks. Elementary blocks like dibenzothiophene, dithienothiophene, carbazole, furan, fluorene, spirofluorene, and fluorenone derivatives, to cite but a few of them, represent ideal functional cores in organic electronic, and can be synthetically or are commercially available now. They thus become ubiquitous for the design and synthesis of novel, low symmetry DLCs for potential uses in various organic electronic-based applications.[4] We have recently developed an efficient strategy based on a tandem of model reactions, namely the $Pd(PPh_3)_4$-catalyzed Suzuki-Miyaura cross-coupling and the $FeCl_3$-catalyzed Scholl oxidative annulation reactions, to construct novel butterfly-like shape molecules showing mesomorphous and promising hole and electron charge carriers behaviors (**DTT**, **CPTO**, Figure 1).[24-26]

The key of this generic methodology for the synthesis of these new ditriphenylenes (**CTP**, **LTP**, **FTP**) lies on the availability of specific carbazole-, fluorene- and fluorenone-containing polybromide precursors and/or corresponding boronic esters (or to a lesser extend their hydroxyl homologs),[27] not always

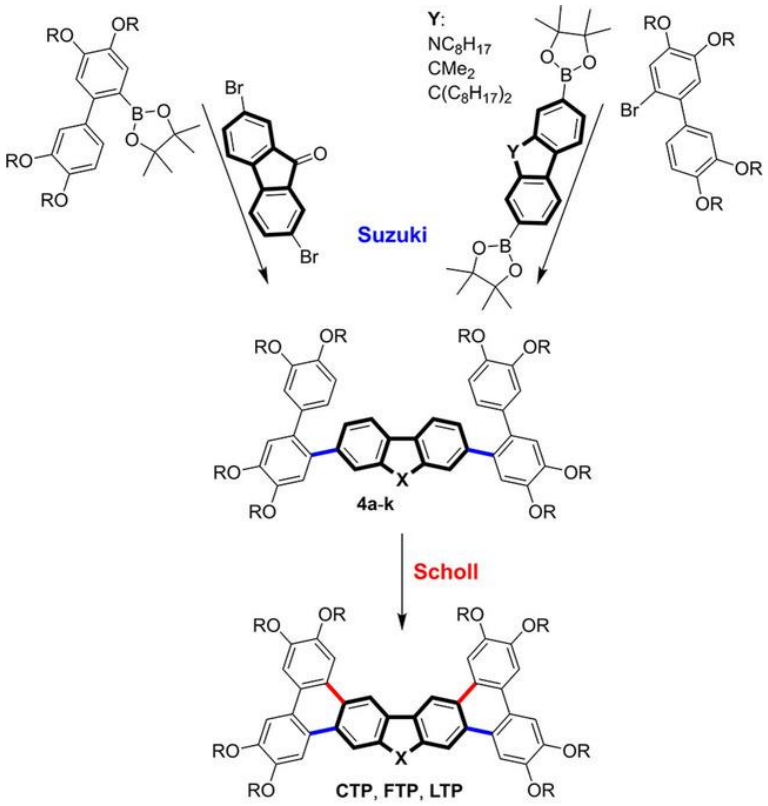

X / n	NC_8H_{17}		CO		CMe_2		$C(C_8H_{17})_2$	
5	-	-	-	-	4e	LTP5	4i	LTP58
8	-	-	-	-	4f	LTP8	4j	LTP88
10	-		4c	FTP10	4g	LTP10	4k	LTP108
12	4a	CTP12	4d	FTP12	4h	LTP12	-	-
14	4b	CTP14	-	-	-	-	-	-

Scheme 1. Synthesis and chart of **CTP**, **FTP** and **LTP** butterflies and precursors. Reaction conditions: Suzuki coupling, $Pd(PPh_3)_4$, K_2CO_3, H_2O/THF, 65 °C; Scholl annulation, $FeCl_3$, $MeNO_2/CH_2Cl_2$. R=C_nH_{2n+1}, with *n*=5, 8, 10,12 and 14. Chemical procedures are detailed in the supporting information.

easily accessible, as reported in Scheme 1. Numerous strategies have been developed for the synthesis of carbazole-based materials and most of them involve bromide derivatives as starting materials. Just to cite but a few, the direct bromination of carbazole results in 1,3,6,8-tetrabromocarbazole, which has been used for the synthesis of some functional 1,3,6,8-tetraarylcarbazole materials.[8, 28] The synthesis of some larger fused π-systems was performed from 2,3,6,7-tetrabromocarbazole and 1,2,3,6,7,8-hexabromocarbazole, however prior required sequential brominations of 2,7-dibromocarbazole (and/or of its N-alkyl derivatives) by precisely controlling bromine concentration, reaction time and temperature.[29] Here, the two novel large N-heteroarene discogenic diphenanthro[9,10-*b* : 9',10'-*h*]carbazoles, **CTP12/14**, were directly synthesized by Suzuki-Miyaura cross-coupling between the commercial *N*-octyl carbazole-2,7-diboronic ester and the alkylated-substituted 2-bromo-1,1'-biphenyl (Scheme S1), subsequently followed by the $FeCl_3$-catalyzed Scholl annulation. The same strategy was followed for the alkyl-substituted fluorene-fused ditriphenylenes (**LTP5/8/10/12/58/88/108**), obtained from the available 9,9-dialkylfluorene-2,7-diboronic esters. The fluorenone-fused ditriphenylenes, **FTP10/12**, were obtained by the inverted alternative, starting with the conversion of the appropriate lipophilic 2-bromo-1,1'-biphenyl into its 1,1'-biphenyl-2-boronic ester first, followed by the subsequent reaction with the commercially available 2,7-dibromo-9-

fluorenone. The oxidative Scholl annulation led to the desired pure compounds, and proceeded in rather satisfying yields (ca. ranging between 47 to 94 %), whereas for the Suzuki coupling reactions, yields were greater than 60–70 % up to quantitative, except for two of them (**4 d**/**e**, Supplementary Information), whose yields were below 50 %, due to purification processes.

All the synthesized ditriphenylene discogens **CTP12**/**14**, **FTP10**/**12**, **LTP5**/**8**/**10**/**12** and **LTP58**/**88**/**108** and precursors (**4 a**–**k**) were fully characterized by ^{1}H NMR and micro elemental analysis, with additional ^{13}C NMR and HRMS for the final target compounds (Figures S1–S43 and S45–S55 in Supporting Information). Among the synthesized discogens, the **CTP** and **FTP** compounds strongly aggregate in solution, due to their low solubility in organic solvents. Their purification was performed by silica gel column chromatography in hot toluene.

Thermal behavior, structural properties, and supramolecular organizations The chemical stability of these molecules was verified by thermal gravimetrical analysis (TGA). All the ditriphenylenes were found to show rather high thermal stability, irrespective of the heteoarenic core, chains' length or topology (linear or bifurcated). The decomposition temperatures at 1 %-, 2 %- and 5 %-weight-loss were systematically higher than 340 °C, 361 °C and 377 °C, respectively (Table S4, Figure S63). Their clearing temperatures were far lower than their thermal decomposition temperatures, so all were candidates for further investigations.

The liquid crystalline properties of the targeted ditriphenylene discogens were studied by polarized optical microscopy (POM, Figure 2 and Figure S62) and differential scanning calorimetry (DSC, Figure 3 and Figure S64, Table S5). As first revealed by POM, the carbazole-, fluorenone- and some of the fluorene-based butterflies are mesomorphous and, as anticipated from other structurally related systems,[24-26] they self-organize into columnar mesophases. POM photographs (Figure 2 and Figure S62) of **CTP12**/**14** and **FTP10**/**12** display the characteristic fan-shaped textures of hexagonal columnar mesophases. When the samples were slowly cooled from the isotropic liquid to the anisotropic state, the compounds held between two glass plates showed birefringent textures with strong tendency for face-on orientation. This typical optical texture originates likely from the strong anisotropy of the supramolecular columns resulting from efficient π-π face-to-face stacking, while the straight defect-lines implied long-range stacking ordering within the columns. The presence of large homeotropic zones in some cases conveys to uniaxial columns orthogonally arranged in hexagonal arrays. An important increase of the mesophase stability by ca. 100 °C is observed on changing from the carbazole-containing compounds (**CTP**) to the fluorenone (**FTP**) derivatives (Figure 3). The carbazole compounds show clearing points of ca. 200 °C and columnar mesophase ranges are about 100 °C large. The fluorenone derivatives display higher clearing temperatures, around ca. 280–300 °C, and mesophases with twice wider ranges, of ca. 210–240 °C, respectively. These observations seem to be in agreement with their respective molecular structures. On the one hand, the presence of the polar ketone group in the π-conjugating core of the fluorenones favors strong antiparallel dipole-dipole interactions in the columnar stacks, whereas the octyl chain irradiating from the carbazole unit, on the other hand, also promoting this antiparallel arrangement, must somehow interfere with the stacking. For the dimethyl fluorene-based derivatives, **LTP5**/**8**/**10**/**12**, POM analysis reveals the absence of mesomorphic behavior for **LTP5**, exhibiting highly colored mosaic texture and straight-line defects, typical of a crystalline phase (Figure S62). However, the other **LTP8**/**10**/**12** compounds with longer linear chains, all exhibit broken fan-shaped, small domains and homeotropic zones in the high temperature mesophase, strongly pointing to the occurrence of a Col_{hex} mesophase as for the carbazole and fluorenone derivatives. On further cooling, the textures change to mosaic-like texture for **LTP8** and needle-like textures for **LTP10** and **LTP12**, indicating the transition to another mesophase of lower symmetry. However, by this technique only, the nature of the mesophases could not be

unequivocally confirmed. The optical textures persist down to low temperatures, particularly for **LTP8**, well below the phase' transition, but signs of crystallization could eventually be observed. The maximum mesophase extension is observed for the decyl homolog, 142 °C for **LTP10**, concomitantly with the decrease of both clearing and melting temperatures (Figure 3). The presence of the two methylene groups lying perpendicularly to the molecular plane must certainly optimize the efficiency of the molecular stacking by locking the antiparallel stacking of the molecules, thus promoting the formation of highly cohesive supramolecular columns organized in mesophases. The substitution of the methylene groups by the two long octyl chains in the **LTP58**/**88**/**108** congeners, although contributing largely to the depression of the melting temperatures by ca. 100 °C, appears however detrimental to the emergence of mesomorphism (Figure S62). The bulky protruding chains lying perpendicularly to the molecular plane in this case likely thwart the efficiency of the molecular stacking, and impact on the phase stability. Of interest, the behavior of these annulated π-extended fluorene molecules is very different from that of recently reported triads made of a fluorene-bridged sigma-bonded with two triphenylene, displaying nematic/columnar mesophases, resulting from the more flexible molecular conformation.[16]

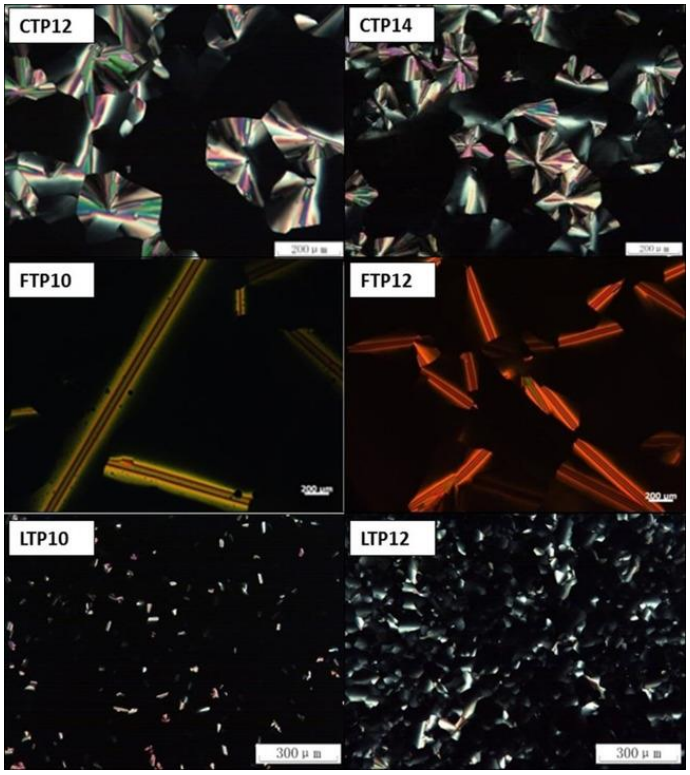

Figure 2. Representative POM images textures of **CTP12** (120 °C), **CTP14** (145 °C), **FTP10** (260 °C), **FTP12** (220 °C), **LTP10** (185 °C) and **LTP12** (180 °C), obtained on slowly cooling from the isotropic liquid. Additional POM images can be found in the Supplementary file (Figure S63).

The transition temperatures were duly confirmed by DSC (Figure S64, Table S5). DSC thermograms also revealed the polymorphic nature of **CTP** and **LTP** compounds. In general, the thermal behavior of all the compounds were found to be fully reversible and reproducible after several heating/cooling cycles, confirming their excellent thermal stability. Notice that another transition was also detected by DSC on cooling only for the **LTP10** homolog, suggesting the induction of a monotropic phase, see below (Figure 3).

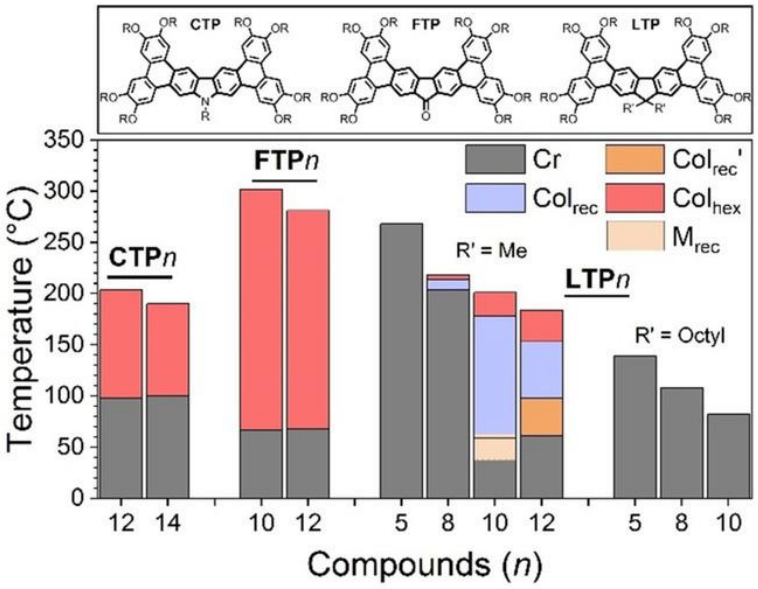

Figure 3. Phase diagram of the fused ditriphenylenes **CTP12/14**, **FTP10/12**, **LTP5/8/10/12** and **LTP58/88/108** (R=C$_n$H$_{2n+1}$). Second heating run shown. Cr: crystalline phase; Col$_{hex}$: hexagonal columnar phase; Col$_{rec}$ and Col$_{rec}$': rectangular columnar phases; M$_{rec}$: monotropic phase with a rectangular 2D symmetry (see S/WAXS analysis for mesophase identification).

The nature of the mesophases and supramolecular organizations of these various butterfly-shaped ditriphenylenes were studied by small- and wide-angle X-ray scattering (S/WAXS, Figure S65, Table S6) and the main geometrical data are summarized in Table 1. The S/WAXS patterns indistinctly possess the characteristic features of liquid-crystalline phases with sharp, small-angle reflections emerging from the nanosegregated structure formed by the antagonistic aromatic and aliphatic segments, along with the scattering signals in the wide-angle region, h_{ch} and h_{π}, emerging respectively from liquid-like lateral distances between molten chains (h_{ch}~4.50–4.80 Å) and from the stacking between the juxtaposed mesogenic cores (h_{π}~3.40–3.90 Å); let us remark that this latter signal is present for almost all compounds, though rather weak for some of them, and systematically decreases until its complete collapsing at or near the clearing temperature (Figure S65).

The assignment of the Col$_{hex}$ mesophase made by POM for **CTP12/14**, **FTP10/12** and **LTP10/12** was unambiguously confirmed by S/WAXS. The presence of one very sharp and intense first-order reflection (10), along one or two weaker, additional higher-order reflections, indexed as (11) and (20), respectively, according to the sequence of spacing ratios 1 : √3 : √4 (Figure 4), confirms the long-range ordering of a two-dimensional hexagonal lattice. The high-temperature mesophase of **LTP8** could only be identified by POM (i. e. Col$_{hex}$, Figure S62) due to its limited temperature range preventing conclusive S/WAXS acquisition. Whereas only one mesophase is formed for both **CTP** and **FTP** compounds, additional mesophases below the Col$_{hex}$ mesophases were detected for the mesomorphous **LTP** homologs. The S/WAXS patterns recorded at these temperatures exhibit a multitude of sharp peaks in the small-angle range (>12, Figure S65 for **LTP8/10/12**), characterizing the formation of mesophases of lower symmetry. In the wide-angle range, the same features as for the Col$_{hex}$ phases discussed above were found, except for the considerable enhancement of the core-core stacking peak's intensity in most cases (h_{π}~3.53–3.64 Å, correlation length ζ~100 for **LTP8** and ζ~115–130 for **LTP12**), evidencing higher overlapping of the extended fluorene cores and the extension of the columnar stacking. The solutions provided by the peaks' indexation (Table S6) convey to 2D rectangular lattices and to the assignment of rectangular columnar mesophases made of two supramolecular columns per lattice. The numerous sharp, small-angle diffraction peaks systematically observed for

these compounds along with the peaks' intensity distribution, reveal the long-range two-dimensional correlated lattices and well defined interfaces, characterized by the efficient segregation between the non-miscible parts, i. e. the supramolecular columns, resulting from the regular stacking of the mesogenic cores localized at the nodes of the lattice, and the molten aliphatic infinite continuum between the columns. Detailed peaks' analysis (Table 1 and Table S6) further indicated two different planar symmetries for the Col_{rec} mesophases i. e. *c*2 *mm* and *p*2*gg*, corresponding respectively to the specific orientations of the elliptical columnar cross-sections within the rectangular lattices, the long elliptical axis lying along the *a*-axis for the centrosymmetric *c*2 *mm* lattice, or alternating its orientation with respect to the same *a*-axis (Figure 4) to form a ribbon-like arrangement for the *p*2*gg* one.[30]

Table 1. Geometrical parameters of the mesophases.

Cpds	T[a]	V_{mol}[b] ρ	Phase[c] Plane group	Mesophase parameters[d] a b	γ	A	Z	A_{mol}[e]	h_{mol}[f] ψ[g]	h_{ch}[h] h_{π}[i]	χ_{core}[j] A_{core}[k]	D_{cyl}/D_{ell}[l] s_{cyl}/s_{ell}[m]	q_{cyl}[n] /q_{ell}
CTP12	180	3824	Col_{hex}	32.24	120	900.1	1	900.1	4.25	4.65	0.179	14.32	1.12
		0.89	*p6mm*	32.24					≈25	3.79	161.1	21.25	
	140	3730	Col_{hex}	32.77	120	930.0	1	930.1	4.01	4.62	0.180	14.6	1.13
		0.91	*p6mm*	32.77					≈20	3.73	167.4	20.44	
	110	3658	Col_{hex}	33.02	120	944.4	1	944.4	3.87	4.57	0.182	14.79	1.13
		0.93	*p6mm*	33.02					≈20	3.68	171.9	19.98	
CTP14	180	4307	Col_{hex}	33.94	120	997.7	1	997.7	4.32	4.68	0.158	14.17	1.11
		0.88	*p6mm*	33.94					≈30	3.81	157.6	21.36	
	160	4254	Col_{hex}	34.77	120	1046.9	1	1046.9	4.06	4.60	0.159	14.56	1.14
		0.89	*p6mm*	34.77					≈20	3.80	166.5	20.65	
	110	4119	Col_{hex}	35.09	120	1066.4	1	1066.9	3.86	4.58	0.161	14.78	1.14
		0.92	*p6mm*	35.09					≈20	3.68	171.8	19.93	
FTP10	250	3258	Col_{hex}	28.54	120	705.6	1	705.6	4.62	4.64	0.223	14.15	0.97
		0.88	*p6mm*	28.54					≈40	3.50	157.3	25.67	
	150	3068	Col_{hex}	29.79	120	768.6	1	768.6	3.99	4.55	0.228	14.93	0.99
		0.94	*p6mm*	29.79					≈30	3.43	175.2	23.41	
FTP12	250	3764	Col_{hex}	30.44	120	802.3	1	802.3	4.70	4.62	0.193	14.04	0.96
		0.86	*p6mm*	30.44					≈40	3.53	154.9	25.87	
	150	3542	Col_{hex}	31.81	120	876.4	1	876.4	4.04	4.45	0.198	14.86	0.99
		0.92	*p6mm*	31.81					≈30	3.43	173.5	23.59	
LTP8	210	2743	Col_{rec}	59.42	90	1558.6	2	779.3	3.52	4.65	0.259	22.67	1.00
		0.92	*p2gg*	26.23					≈0	3.64	201.8	24.16	
LTP10	60	2945	M_{rec}	56.25	90	1726.9	2	863.4	3.41	4.64	0.227	22.34	1.05
		0.98	–	30.70					≈0	3.55	196.0	23.07	
	130	3081	Col_{rec}	57.06	90	1701.5	2	850.8	3.62	4.70	0.223	21.98	1.05
		0.94	*p2gg*	29.92					≈0	3.59	189.7	24.10	
	200	3217	Col_{hex}	31.94	120	883.4	1	883.4	3.64	4.86	0.220	15.73	1.07
		0.90	*p6mm*	31.94					≈0	3.78	194.4	22.49	
LTP12	70	3411	Col_{rec}	61.58	90	2076.5	2	1038.2	3.29	4.65	0.197	22.82	1.03
		0.96	*p2gg*	33.72					≈0	3.53	204.5	22.70	
	120	3524	Col_{rec}	66.6	90	2107.9	2	1053.9	3.34	4.60	0.194	22.82	1.01
		0.93	*c2mm*	31.65					≈0	3.57	204.5	23.10	
	180	3661	Col_{hex}	33.62	120	979.2	1	978.9	3.74	4.60	0.191	15.43	1.05
		0.89	*p6mm*	33.62					≈0	3.80	186.9	22.66	

[a] T, temperature of the S/WAXS measurement (°C); [b] V_{mol}, molecular volume (Å^3) and ρ, density (g.cm^{-3}); [c] phase type and symmetry: Col_{hex}-*p6 mm*, hexagonal columnar phase, Col_{rec}-*c2 mm*/*p2gg*: rectangular columnar mesophase, M_{rec}: mesophase with quasi -rectangular symmetry; [d] a, b, γ, Z: mesophases' lattice parameters (Å and °) and number of columns per lattice; A, lattice area (Å^2) $A = a^2\sqrt{3}/2$ for Col_{hex} phase, and $A = ab$ for rectangular phases; [e] A_{mol}: columnar cross-sectional area (Å^2) $A_{mol} = A/Z$; [f] h_{mol}, molecular slice thickness (Å), $h_{mol} = V_{mol}/A_{mol}$; [g] ψ, out-of- plane tilt angle of mesogen cores inside columns; [h] h_{ch}, lateral distances between molten chains from WAXS pattern; [i] h_{π}, stacking distance from WAXS pattern (Å); [j] core volume fraction, $\chi_{core} = 1-\chi_{ch}$, where $\chi_{ch} = V_{ch}/V_{mol}$ (V_{ch}, aliphatic chain volume fraction); [k] $A_{core} = \chi_{core}A/Z$, circular/elliptical core cross-sectional area (rigid part); [l] diameter of equivalent cylindrical cross-sectional area (A_{core}) for hexagonal phase, $D_{cyl} = \sqrt{(4 \times A_{core}/\pi)}$; diameters at equator ($D_{ell}$) and at poles ($D'_{ell}$) of equivalent ellipse of cross-sectional area (A_{core}) for rectangular phases; from modelling, in a first approximation, $D_{ell} \approx 2D'_{ell}$, and thus $D_{ell} = \sqrt{(8 \times A_{core}/\pi)}$; [m] cross-sectional area per chain for Col_{hex}: $s_{cyl} = \pi D_{cyl} \times h_{mol}/n_{ch}$, where n_{ch} being the number of chains per molecule; for the rectangular phases, the ellipse perimeter was deduced from the Ramanujan first approximation and thus, for $D_{ell} = 2D'_{ell}$, $s_{ell} = (9-\sqrt{35}) \times [\pi D_{ell} \times h_{mol}]/4n_{ch}$; [n] chain packing ratio: $q_{cyl/ell} = s_{cyl/ell}/\sigma_{ch}$, σ_{ch} being the cross-sectional area of a molten chain.[32] See graph of the variation of q_{ell} as a function of D_{ell} in Figure S66.

As shown by DFT calculations (Figure S57), and similarly to other structurally related compounds,[24-26] all these new butterfly-like molecules are planar irrespective of the nature of the central core, suggesting an easy stacking along the columnar axis. Furthermore, these calculations also reveal that their rigid aromatic core adopt an elliptical shape, with a core aspect ratio of almost 2 (i. e. as roughly estimated by the quotient D_{ell}/D'_{ell}, diameter at equator/diameter at the poles, Table 1). The emergence of the hexagonal symmetry implies that the columns must exhibit a time-averaged circular cross-section which allows a homogeneous distribution of the aliphatic chains in the periphery. And indeed, the shape of the core/chain interface of the columns can take the shape of a cylinder by the

continuous orientational change of the pseudo-elliptical mesogens along the stacking direction, with, if necessary, some tilt of the cores with respect to the lattice plane.[31]

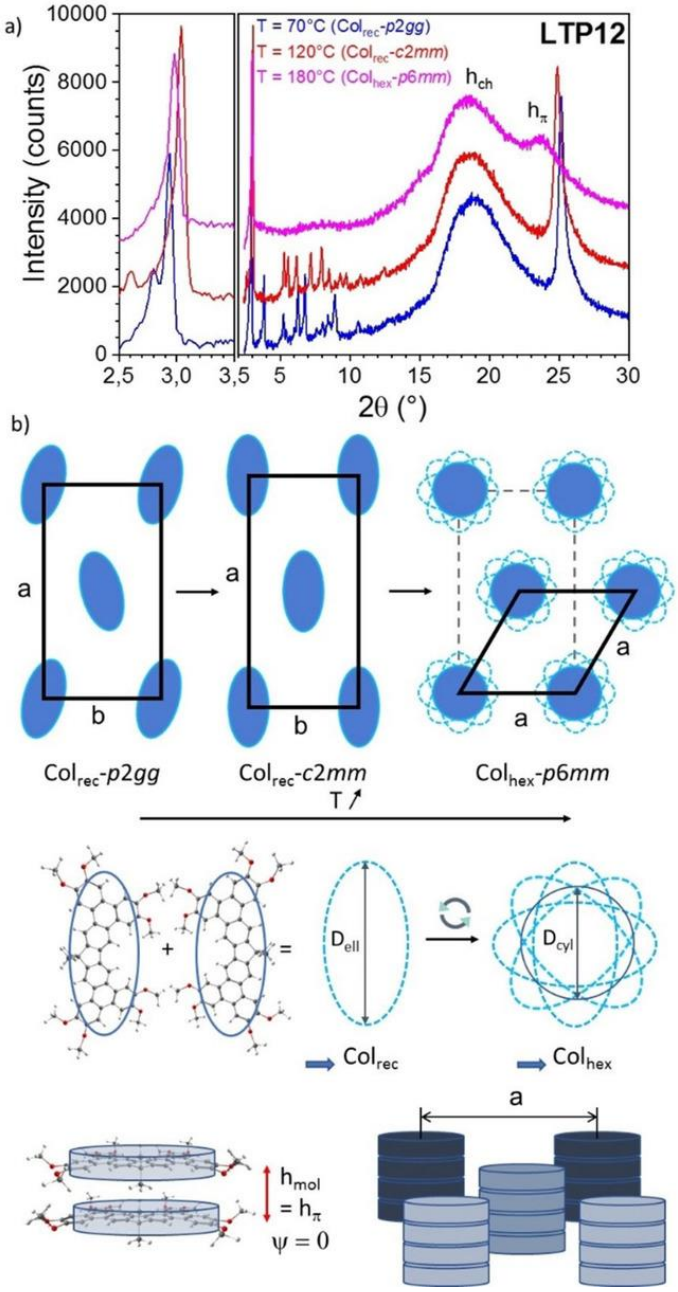

Figure 4. a) Small- and wide-angle X-ray scattering (S/WAXS) patterns of the three mesophases of **LTP12** compound (chosen as a representative example) recorded on cooling at various temperatures. b) Evolution of the lattices' symmetry of the various mesophases of **LTP12** as a function of temperature. Supramolecular organization in the Col_{rec} and Col_{hex} phases: the elongated shape of the aromatic core roughly approximates an ellipse of aspect ratio close to 2 with an interface area per peripheral chain s_{ell}; the ellipses adopt alternated orientations with respect to a-axis (*p2gg*) or are collinear to a-axis (*c*2 *mm*); the random orientational changes of the stacked cores, distribute the space-demanding radiating alkyl chains over the whole stack periphery and design average cylindrical columns of reduced statistical interface area s_{cyl}; elliptical and cylindrical columns arranging in rectangular and hexagonal lattices, respectively of parameter *a* and with molecular slice thickness h_{mol} compared to π-stacking distance, h_{π}.

In all the Col_{hex} mesophases, the area needed by the peripheral chains is highly compatible with the interface area offered by the stacked mesogens, since the ratio q_{cyl} (Table 1) does not deviate much

from unity (<10 % for **CTP** and **FTP** compounds).[32] The chains are therefore stretched and densely packed, allowing for facile orientational changes between neighboring molecules within and, obviously, between columns, resulting in the homogeneous distribution of the aliphatic chains at the periphery of the columns. The values of the molecular slices' thicknesses, h_{mol}, deduced from the ratio between the molecular volume and the columnar area, are almost similar to those of h_{π} (h_{mol} being slightly greater than h_{π}, Table 1) for **CTP** and **FTP** derivatives or identical to the stacking distance ($h_{mol} \approx h_{\pi}$, $\psi \approx 0$) for the **LTP** compounds, equivalent to a non-tilted stacking of the cores along the columnar axis for the latter. In order to manage the even distribution of the central protruding chain in the **CTP** compounds or the carbonyl fragment in the **FTP** ones, the molecules must therefore stack into columns with some small tilts ($\psi \approx 20–30$ for **CTP** and 30–40 for **FTP**, Table 1). These models (Figure 4) are in agreement with the high mesophase stability observed in these series of compounds.

The induction of the rectangular phase for the **LTP** systems is not in contradiction with the above, and the respective orientational changes between juxtaposed molecules must be somehow hindered by the presence of the two diverging methyl group that likely lock the molecules in a specific antiparallel arrangement. These features hamper the easy orientational changes along the piles of the π-stacked mesogens as the temperature is decreased and thus naturally lead to columns with an elliptical cross-section that arrange in a columnar phases of lower symmetry. The ratios between the molecular volume versus the area of the cell (Z=2) provide values for h_{mol} that do not diverge from h_{π}, consistent with orthogonal stacking ($\psi \approx 0$). The area needed by the peripheral chains is also perfectly compatible with the interface area offered by the stacked mesogens, since the ratio q_{ell} (Table 1) is almost equal to unity for an elliptical columnar cross-section of aspect ratio 2. The variation of this ratio as a function of the grand elliptical diameter D_{ell}, comprised between ca. 11 and 24 nm, is comprised between.0.9–1.05, highly compatible with the dimensions of the fluorene core (Table 1, Figure S66). The transition between Col_{rec} and Col_{hex} mesophases in these **LTP** compounds is thus due to both orientational and translational changes of the stacked mesogenic parts along the columnar axis.

Optical physical property Carbazole, fluorene and fluorenone are ubiquitous building blocks in electronic materials used for OLEDs, OPVs, and OFETs[2-4] and the optical properties materials containing these active units determine their future performances in optoelectronic devices.

The UV-vis absorption and photoluminescence of the different butterfly-like mesogens were measured in solution and films. For all, the π-extension increases the UV-vis absorption spectra to 400 nm, and for **FTP** to almost 500 nm, resulting from π-π*, and intramolecular charge transfer (ICT) absorption (Table S1, Figure 5 and Figure S56), independently of the chains' length. All these ditriphenylene compounds also emit in both solution and in thin films. The **CTP** compounds dissolved in THF emit blue light in 430–550 nm with quantum yield (QY) of 26–27 %, and the emission is slightly red-shifted (ca. 10 nm) in the film. All the **LTP** compounds show photoluminescence of blue light in the 360–520 nm range, with outstanding QY of 70 %, while the film fluorescence red-shifts by ca. 62 nm. On the other hand, **FTP** compounds photo-luminesce with orange-yellow light between 480 and720 nm in THF, with absolute QY around 21–28 %, the fluorescence of the film being red-shifted by 61 nm compared with the emission in solution. The topology of the chain affects the film luminescence profile and λ_{em} (Table 2, Figure S56). Usually polycyclic aromatic hydrocarbons (PAHs) exhibit diminished fluorescent efficiency due to extended π-conjugation and aggregation in solution. However, the annulated ditriphenylene derivatives **LTP** show very high QY of 70 % due to the lateral substituted dimethyl/dioctyl of fluorene core, which have potential application as fluorescent sensor and OLED materials. The blue-colored photoluminescence of **CTP** and **LTP** in solution and thin-film implied that these materials can be used in blue-light emitting OLED, as well as in electron-transport materials.[5, 6]

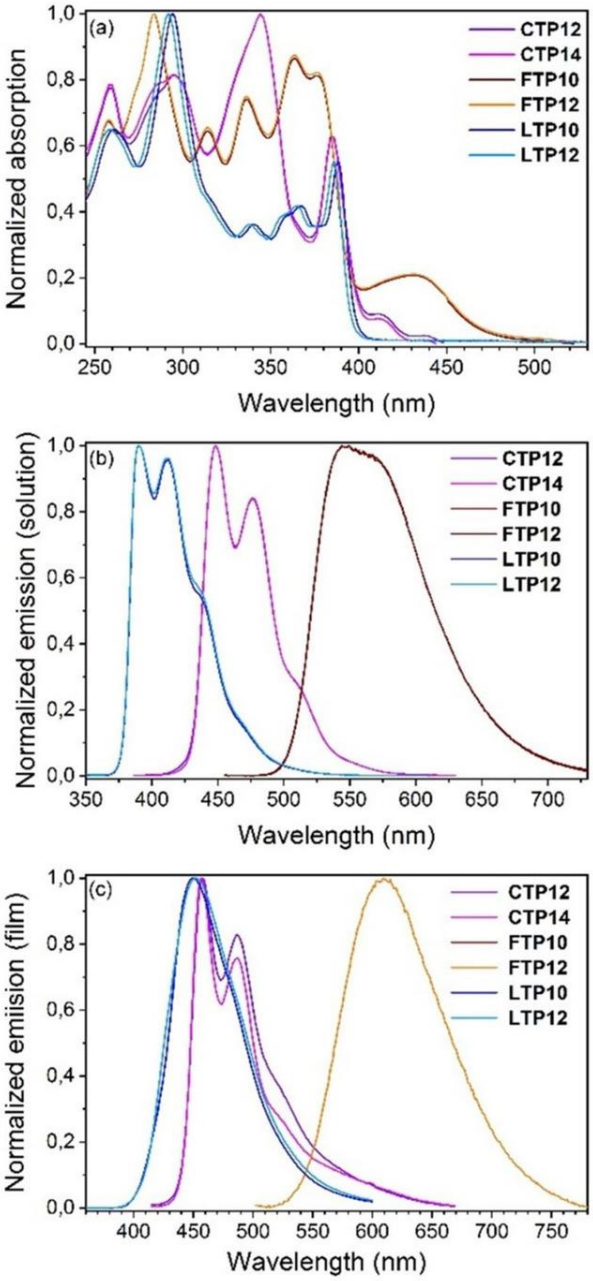

Figure 5. (a) and (b) UV-Vis absorption and fluorescent spectra, measured in THF solutions at a concentration of 1×10^{-5} mol/L with excitation of 365 nm for **CTP**, and 370 nm for **FTP**; at a concentration of 1×10^{-6} mol/L with excitation of 300 nm for **LTP**; (c) photoluminescence of thin-films, measured at 25 °C.

Table 2. Summary of the photoluminescence properties of **CTP**, **FTP** and **LTP** compounds in solution and hot melt films (Complete data in Supplementary Information, Table S1).

Compounds	λ_{em} solution [nm]	QY [%]	λ_{em} film [nm]
CTP*n*	449/476	26.12–27.26	458/486
FTP*n*	548	20.85–27.98	609
LTP*n*	392–393/413–415	69.87–75.26	465

Molecular engineering of this semiconducting butterfly-shape coplanar ditripheylene DLCs effectively modulates the absorption and emission properties, HOMO/LUMO energy levels and energy gaps. The

ground-state molecule geometries and the frontier molecular orbitals were calculated for these three compounds by density functional theory (DFT) at the level of B3LYP-D3/6-311 ++G (d,p) (Figure 6). The calculated HOMO/LUMO levels are −5.31 eV/−1.86 eV, −5.73 eV/−2.75 eV and −5.54 eV/−1.83 eV for **CTP**, **FTP** and **LTP**, respectively. These theoretical results agreed well with the experimental UV-Vis absorption and luminescence spectroscopies. As expected, **FTP** showed downshifted HOMO/LUMO levels and narrower energy gap than **CTP** and **LTP** derivatives, resulting from the introduction of electron-withdrawing ketone unit in the central part. Furthermore, the **FTP**'s HOMO shows the electron density localized mainly on the two tetraalkoxy-triphenylene cores whereas for the LUMO, the electrons are distributed on the central fluorenone core. The more obvious intramolecular charge transfer (ICT) absorption of **FTP** was demonstrated by the contrast HOMO/LUMO wavefunction distribution in theory, and the red-colored sample (organogel) and red-shifted solution/aggregation emission in experiments.

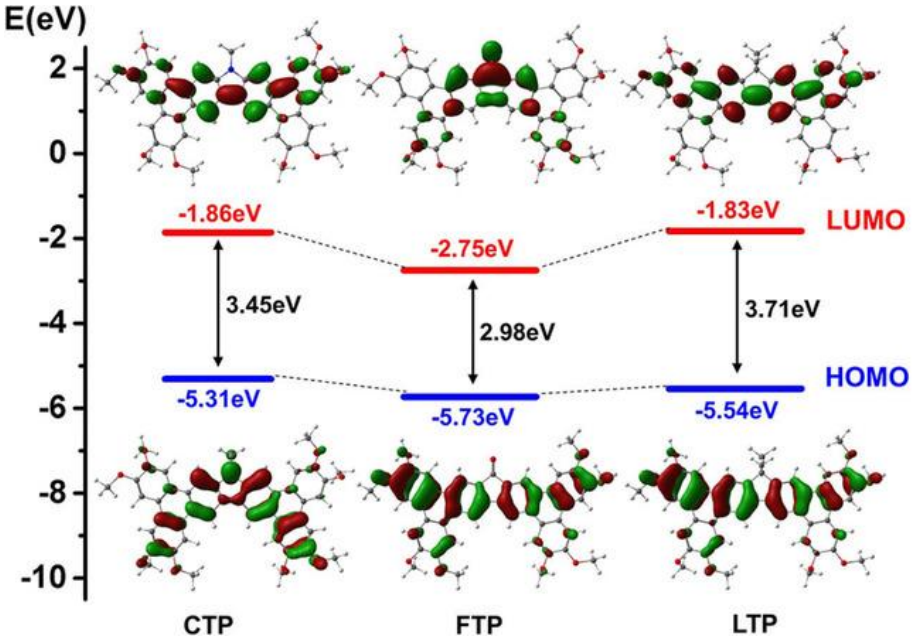

Figure 6. Calculated molecular frontier orbitals and energy levels for **CTP**, **FTP** and **LTP** homologs with methoxy radicals (More detailed diagrams of the HOMO-LUMO frontier orbitals can be found in Supporting Information).

Gelling properties Organic gelators possessing very strong intermolecular interactions, such as π-π, dipole-dipole, or hydrogen bond can lock enough solvent molecules to form organic gels. Supramolecular gelators further tend to self-assemble into intricate 3D-networks made of nano- to micro-fibers, rods, tubes or bands.[33] The present fused ditriphenylenes are extended π-conjugated aromatics with long peripheral alkyl chains, and are thus expected to also aggregate in organic solvents and thus to be good candidates as π-gelators. To test their gelling abilities, a fixed amount of the sample was dissolved in different solvents by heating until complete dissolution and then were slowly cooled down. The formation of the organogels was confirmed by the "stable to inversion of the test tube" method (Figure 7 and Figure S59). The gel-forming of **CTP12** and **LTP10** compounds are summarized in Table 3. We found that indeed the **CTP** and **FTP** mesogens aggregate in organic solvents and show good gelling properties. In contrast, the fluorene derivatives **LTP** do not aggregate in solution as evidenced from the invariance of the ^{1}H NMR spectra aromatic signals with increasing concentration (Figure S44), and as result do not form gels. The presence of the chains at the tip of the fluorene core radiating out of the molecular plane (Figure S57), may disturb efficient π-π intermolecular interactions in solution and be responsible for the increase solubility in the solvents, consequently reducing its gel-forming tendency.

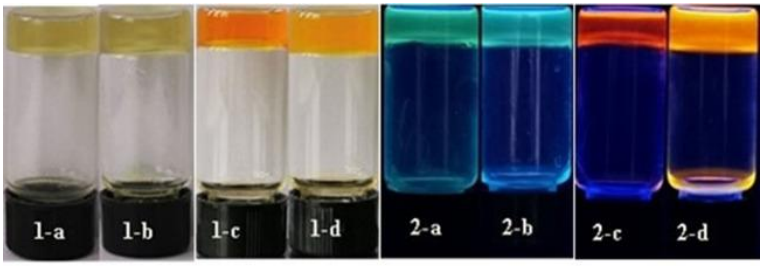

Figure 7. Gelation of **CTP12** and **FTP10** in various organic solvents: **CTP12** in hexane (a) and cyclohexane (b); **FTP10** in CH_2Cl_2 (c) and THF (d). Pictures of the gels in day light, 1-a/d, and the corresponding images under UV light (365 nm) 2-a/d.

Table 3. Gelation properties of two representative synthesized π-gelators in organic solvents.[a,b,c]

Solvent	CTP12	FTP10
Hexane	G(3)o	G(2)o
Cyclohexane	G(3)o	G(2)o
Toluene	S	G(2)t
CH_2Cl_2	S	G(2)t
$CHCl_3$	S	G(5)t
THF	S	G(3)o
Ethanol	I	I

[a] G, S and I indicate the state of the mixture when heated, corresponding to gel, solution and insoluble, respectively. [b] The numbers in brackets correspond to the critical gelation concentration (CGC) in mg mL^{-1}. [c] o and t denoted the appearance of the gel: o, opaque gel; t, transparent gel.

CTP12 can form organogel in nonpolar organic solvents such as hexane or cyclohexane, in concentration of 3.0 mg mL^{-1} (Figure 7). It also dissolves in hot polar solvents such as CH_2Cl_2 and $CHCl_3$, but precipitates on cooling without forming gels. These gels emit blue-light under UV irradiation. **FTP10** displays stronger gelling ability than **CTP12**, locking both nonpolar solvents (hexane, cyclohexane, toluene) and polar solvents (CH_2Cl_2, $CHCl_3$, THF) at much lower concentrations, of 2.5 mg mL^{-1} (Figure 7 and Figure S59). They emit strong yellow light under UV irradiation.

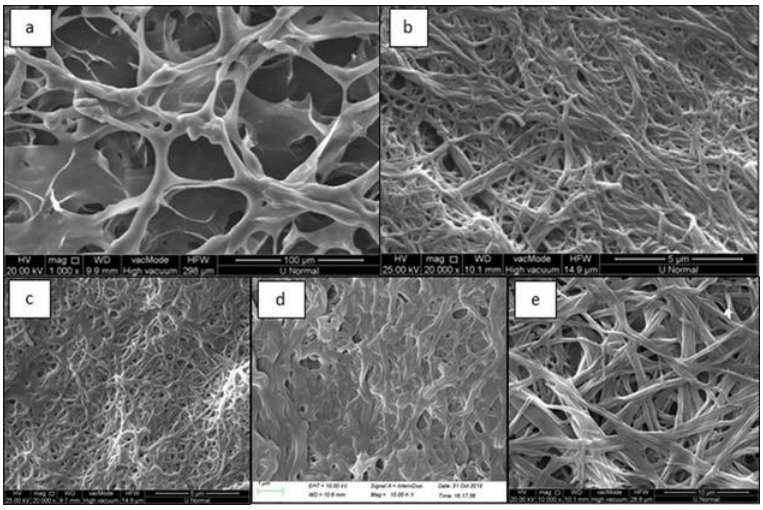

Figure 8. SEM images of xerogels of: (a) **CTP12** in cyclohexane; (b) **FTP-10** in hexane; (c) **CTP12** in toluene/EtOH ("good"/"poor" solvent); (d) **FTP10** in toluene/EtOH ("good"/"poor" solvent); (e) **LTP10** in CH_2Cl_2/EtOH ("good"/"poor" solvent). Other SEM images are shown in Figures S60-S61.

As revealed by SEM, the morphology of the xerogel formed by **CTP12** in apolar solvents showed densely packed 3D networks, composed of entangled nanofibrous structures with lengths of more than several micrometers and width of a few tens of micrometers (Figure 8a and Figure S60). For **FTP10**, both 3D networks of interwoven nanofibres and long helicoidal fibers are formed (Figure 8b and Figure S60), though the fibers appear much thinner than those in **CTP12** xerogels, irrespective of the solvents. Interestingly, in mixed solvents, containing "good" (toluene) and "poor" (ethanol) solvents, it was found that each representative compound, including **LTP10** (using dichloromethane instead of toluene) aggregates, and exhibits stable, complex networks of intermingled long fibers (Figure 8c-e and Figure S61).

Semiconducting Properties Self-organized columnar nanostructures consisting of two π-extended polycyclic aromatic hydrocarbons connected with carbazole, fluorene, and fluorenone moieties can be imagined as potentially microscopic supramolecular cables for charge carrier hopping pathways. Transient photocurrent time-of-flight (TOF) technique is a unique, accurate, direct and relatively simple method to measure charge carrier mobility of organic semiconductors with a very long charge hopping pathway through a distance of 15 to 20 μm along the π-π overlapping columns stacked by thousands of columnar molecules, very similar to their situations in electronic devices (from a few μm to 50 μm). We have investigated the photoconductive properties of four synthesized columnar mesogens with carbazole, fluorene, and fluorenone as central linking cores, respectively, by using the above mentioned TOF method, and the results are showed in Figure 9, and in more detail in supplementary information (Figures S67–S76 and Tables S7–S13).

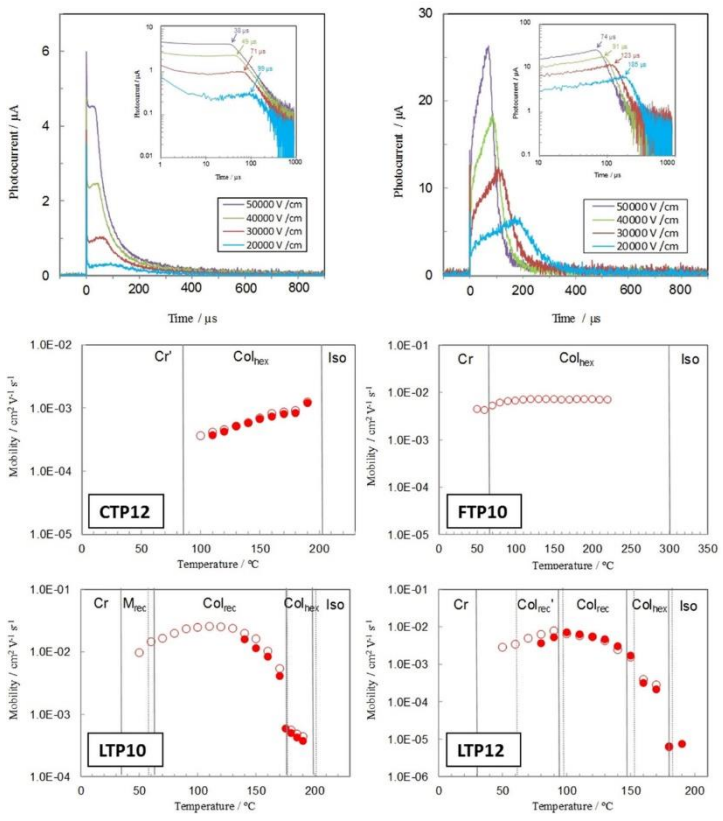

Figure 9. (Top) Samples of transient photocurrent decay curves of hole on cooling run in the Col_{hex} phases for **CTP12**, at 160 °C, and for **LTP10**, at 190 °C; the insets show log-log plot, and the transit time at various electric field (2–5×10^4 Vcm^{-1}) was labeled. (Bottom) Temperature dependence of charge carrier mobility for **CTP12**, **FTP10**, **LTP10**, and **LTP12** on cooling (open circle) and heating (close circle).

The transient photocurrent decay curves are all in good shape and non-dispersive, demonstrating the high purity of these molecular semiconductors and thermal stability and excellent homeotropic alignment behavior in ITO cells. **CTP12** with carbazole linkage shows a hole mobility of ca. 1.3×10^{-3} $cm^{-2}\,V^{-1}\,s^{-1}$ at 190 °C in the Col_{hex} phase, which substantially decreases to 4.2×10^{-4} $cm^{-2}\,V^{-1}\,s^{-1}$ on cooling, within the same range of 10^{-4}–10^{-3} $cm^{-2}\,V^{-1}\,s^{-1}$ exhibited by the well-known triphenylene discogens,[34] reflecting the formation of fairly ordered 1D π-stacked nanostructures in the Col_{hex} phase. The photoconductive mobility of **CTP12** was fully reversible in successive heating and cooling runs, demonstrating that this carbazole-connected triphenylenes core is a good semiconducting columnar mesogen. On the contrary, **FTP10** with a fluorenone linkage which has less alkyl chain in the core part shows higher hole mobility rate than **CTP12**, with a value of ca. 7.3×10^{-3} $cm^{-2}\,V^{-1}\,s^{-1}$ over the entire mesomorphic range (Col_{hex}) in the cooling cycle, decreasing down to 4.3×10^{-3} $cm^{-2}\,V^{-1}\,s^{-1}$ at the transition to the crystalline phase. Both **LTP10** and **LTP12** compounds, with fluorene linkage, show low hole mobility values of ca. $(4.4–5.6)\times10^{-4}$ $cm^{-2}\,V^{-1}\,s^{-1}$ and $(2.9–4.0)\times10^{-4}$ $cm^{-2}\,V^{-1}\,s^{-1}$, respectively, in the high temperature Col_{hex} phase. However, on cooling in the Col_{rec} phases, the hole mobilities rise and reach 2.6×10^{-2} $cm^{-2}\,V^{-1}\,s^{-1}$ and 6.5×10^{-3} $cm^{-2}\,V^{-1}\,s^{-1}$ at 110 °C and 100 °C, respectively. On subsequent cooling **LTP10** and **LTP12** in the lower temperature M_{rec} and Col_{rec}' phases, the hole mobilities decrease to 9.8×10^{-3} $cm^{-2}\,V^{-1}\,s^{-1}$ and 2.9×10^{-3} $cm^{-2}\,V^{-1}\,s^{-1}$, respectively, probably due to the charge trapping at grain boundary in poly domains of the highly ordered columnar mesophase.

In summary, these novel ditriphenylene columnar mesogens from carbazole, fluorenone, and fluorene show outstanding charge carrier transport properties mainly due to their larger π-electron systems especially for those fused with fluorenone and fluorene. The other factors contributing to the outstanding high TOF positive charge carrier mobility of **LTP10/12** compared with other discotic mesogens[35, 36] may include their higher ordered rectangular columnar (Col_{rec}) mesophase (demonstrated by S/WAXS and POM results), as well as the decreased intracolumnar molecular dynamics by the lateral substitution of dimethyl groups on the fluorene core.

Conclusions

Several butterfly-shaped columnar liquid crystals featuring two triphenylenes fused with a central carbazole, fluorenone, and fluorene molecular moiety, respectively, have been synthesized. Their facile and straightforward synthetic strategy was accomplished by the Suzuki-Miyaura cross-coupling and Scholl oxidative cyclodehydrogenation tandem reactions. The polar **CTP** and **FTP** series display a single and broad mesophase, Col_{hex}, with very high clearing temperatures. The dimethyl terms of the **LTP** series show a rich self-organizational behavior including both rectangular (Col_{rec}) and hexagonal (Col_{hex}) columnar mesophases. **CTP** and **LTP** in solution exhibit blue-light photoluminescence with absolute quantum yield of 27 % and 70 % respectively; while **FTP** solution emits yellow-light due to the intramolecular charge transfer (ICT), with absolute quantum efficiency of 28 %. **CTP** forms organogel in non-polar solvents; while polar mesogens **FTP** strongly gelate both polar and non-polar organic solvents; however, **LTP** cannot form organo-gel in in single solvent, but entangled fibrous networks emerged in mixture of good/poor solvents. Photocurrent time-of-flight results show that all compounds display hole mobility. In particular, **LTP** compounds show a hole mobility jump from $(4.4–5.6)\times10^{-4}$ $cm^2\,V^{-1}\,s^{-1}$, in the Col_{hex}, up to almost 0.03 $cm^2\,V^{-1}\,s^{-1}$ (**LTP10**) in the lower temperature higher ordered phase, due to large π-π overlaps.

We believe that this generic synthetic strategy can be applied to other suitable electronically active molecular blocks in order to ease the construction and expand further the growing variety of more

complex annulated π-extended optoelectronic materials with potential applications in various electronic film devices.

Experimental Section

All solvents and commercial reagents were used without further purification. The synthesis of the precursors (**1 a**–**e**, **2 a**–**e**, **3 a**–**b**, and **4 a**–**k**, Scheme 1 and Scheme S1) and characterization (NMR, Figures S1–S43, HRMS, Figures S45–S55) are shown in the supplementary information.

(**CTP12**) 10-Octyl-2,3,6,7,13,14,17,18-octakis(dodecyloxy)-10*H*-diphenanthro[9,10-*b* : 9',10'-*h*]carbazole. To a 100 mL round bottom flask, **4 a** (0.18 g, 0.09 mmol), then $FeCl_3$ (0.09 g, 0.52 mmol) in dichloromethane (60 mL) and nitromethane (5 mL) were added, and stirred at room temperature. The reaction was tracked every 15 minutes. When the reaction was finished, the mixture was quenched by addition of cold methanol. Then, it was extracted with dichloromethane, dried over $MgSO_4$, filtered and solvent removed by rotary evaporation. Purification with silica gel column chromatography (toluene/petroleum ether=1 : 1 v/v) and recrystallization with ethanol and ethyl acetate gave a yellow-green solid, **CTP12** (0.09 g, 50 %). ^{1}H NMR ($CDCl_3$, TMS, 400 MHz) δ (ppm): 9.34 (s, 2H, ArH), 8.33 (s, 2H, ArH), 8.29 (s, 2H, ArH), 8.15 (s, 2H, ArH), 7.88 (s, 4H, ArH), 4.58–4.61 (m, 2H, NCH_2), 4.37–4.42 (m, 4H, OCH_2), 4.25–4.33 (m, 12H, OCH_2), 1.96–2.14 (m, 18H, CH_2), 1.62–1.67 (m, 12H, CH_2), 1.25–1.45 (m, 142H, CH_2),0.87 (t, *J*=8.0 Hz, 27H, CH_3). ^{13}C NMR ($CDCl_3$, TMS, 100 MHz) δ (ppm): 149.72, 149.21, 148.87, 148.78, 141.75, 128.59, 125.06, 127.71, 124.10, 123.19, 123.09, 122.33, 114.59, 108.49, 108.14, 107.63, 107.29, 100.31, 70.17, 70.02, 69.78, 69.58, 31.94, 31.82, 29.80, 29.76, 29.73, 29.71, 29.67, 29.63, 29.62, 29.59, 29.50, 29.44, 29.40, 29.31, 28.63, 27.52, 26.30, 26.26, 22.70, 22.63, 14.12, 14.04. HRMS m/s (MALDI): $[M]^{+\cdot}$ Calcd. for $C_{140}H_{229}NO_8$: 2053.7577; Found: 2053.7578. Elemental analysis: Calcd. for $C_{140}H_{229}NO_8$: C 81.85 %, H 11.24 %, N 0.68 %; Found: C 81.94 %, H 11.30 %, N, 0.30 %.

(**CTP14**) 10-Octyl-2,3,6,7,13,14,17,18-octakis(tetradecyloxy)-10*H*-diphenanthro[9,10-*b* : 9',10'-*h*]carbazole. As above. (**4 b**) (0.21 g, 0.09 mmol), $FeCl_3$ (0.09 g, 0.55 mmol) in dichloromethane (60 mL) and nitromethane (5 mL). Purification by silica gel column chromatography (toluene/petroleum ether=1 : 1 v/v) and recrystallization with ethanol and ethyl acetate resulted in a yellow-green solid **CTP14** (0.1 g, yield 47 %). ^{1}H NMR ($CDCl_3$, TMS, 400 MHz) δ (ppm): 9.32 (s, 2H, ArH), 8.32 (s, 2H, ArH), 8.27 (s, 2H, ArH), 8.13 (s, 2H, ArH), 7.87 (s, 4H, ArH), 4.55–4.58 (m, 2H, NCH_2), 4.42 (t, *J*=8 Hz, 4H, OCH_2), 4.25–4.31 (m, 12H, OCH_2), 2.10–2.13 (m, 2H, CH_2), 1.98–2.03 (m, 16H, CH_2), 1.69–1.67 (m, 18H, CH_2), 1.25–1.46 (m, 168H, CH_2), 0.87 (t, *J*=8 Hz, 27H, CH_3). ^{13}C NMR ($CDCl_3$, TMS, 100 MHz) δ (ppm): 149.77, 149.26, 148.91, 148.33, 141.77, 128.62, 125.09, 124.75, 124.15, 123.21, 123.13, 122.36, 114.60, 108.60, 108.24, 107.73, 107.39, 100.33, 70.20, 70.06, 69.82, 69.62, 31.92, 31.81, 29.79, 29.77, 29.74, 29.72, 29.70, 29.68, 29.65, 29.61, 29.60, 29.58, 29.51, 29.43, 29.37, 29.29, 28.62, 27.51, 26.29, 26.25 22.68, 22.61, 14.09, 14.01. HRMS m/s (MALDI): $[M]^{+\cdot}$ Calcd. for $C_{156}H_{261}NO_8$: 2278.0081; Found: 2278.0078. Elemental analysis: Calcd. for $C_{156}H_{261}NO_8$: C 82.22 %, H 11.55 %, N 0.61 %; Found: C 81.98 %, 11.22 %, N, 0.30 %.

(**FTP10**) 2,3,6,7,12,13,16,17-Octakis(decyloxy)-20*H*-cyclopenta[1,2-*b* : 3,4-*b*']ditriphenylen-20-one. As above. **4 c** (0.11 g, 0.07 mmol), $FeCl_3$ (0.06 g, 0.39 mmol), in chloroform (60 mL) and nitromethane (5 mL). Silica gel column chromatography (toluene/petroleum ether=1 : 2 v/v). Recrystallization toluene and petroleum ether gave an orange-yellow solid **FTP10** (0.09 g, 80 %). ^{1}H NMR ($CDCl_3$, TMS, 400 MHz) δ (ppm): 8.35 (s, 2H, ArH), 8.18 (s, 2H, ArH), 7.91 (s, 2H, ArH), 7.56 (s, 2H, ArH), 7.43 (s, 2H, ArH), 7.41 (s, 2H, ArH), 4.36 (t, *J*=8.0 Hz, 4H, OCH_2), 4.10 (t, *J*=4.0 Hz, 12H, OCH_2), 1.92–2.07 (m, 16H, CH_2), 1.62–

1.72 (m, 10H, CH_2), 1.25–1,48 (m, 102H, CH_2), 0.90 (t, *J*=8.0 Hz, 24H, CH_3). HRMS m/s (MALDI): $[M]^{+\cdot}$ Calcd. for $C_{117}H_{180}O_9$: 1730.3661; Found: 1730.3660. Elemental analysis: Calcd. for $C_{117}H_{180}O_9$: C 81.20 %, H 10.48 %; Found: C 80.96 %, H 10.59 %.

(**FTP12**) 2,3,6,7,12,13,16,17-Octakis(dodecyloxy)-20*H*-cyclopenta[1,2-*b* : 3,4-*b*']ditriphenylen-20-one. As above. **4 d** (0.14 g, 0.07 mmol), $FeCl_3$ (0.07 g, 0.43 mmol) in chloroform (60 mL) and nitromethane (5 mL). Silica gel column chromatography (toluene/petroleum ether=1 : 2 v/v). Recrystallization from ethyl acetate and ethanol (toluene and petroleum ether) gave an orange-yellow solid **FTP12** (0.07 g, 47 %). ^{1}H NMR ($CDCl_3$, TMS, 400 MHz) δ (ppm): 8.41 (s, 2H, ArH), 8.24 (s, 2H, ArH), 7.94 (s, 2H, ArH), 7.61 (s, 2H, ArH), 7.47 (s, 2H, ArH), 7.45 (s, 2H, ArH), 4.37 (t, *J*=8.0 Hz, 4H, OCH_2), 4.09–4.15 (m, 12H, OCH_2), 1.94–2.05 (m, 16H, CH_2), 1.61–1.70 (m, 16H, CH_2), 1.30–1,45 (m, 128H,CH_2), 0.89 (t, *J*=8.0 Hz, 24H, CH_3). HRMS m/s (MALDI): $[M+H]^{+\cdot}$ Calcd. for $C_{133}H_{212}O_9$: 1955.6243; Found 1955.6264. Elemental analysis: Calcd. for $C_{133}H_{212}O_9$: C 81.71 %, H 10.93 %; Found: C 82.06 %, H 11.23 %.

(**LTP5**) 2,3,6,7,12,13,16,17-Octakis(pentyloxy)-20,20-dimethyl-20*H*-cyclopenta[1,2-*b* : 3,4-*b*']ditriphenylene. As above. **4 e** (0.1 g, 0.08 mmol), dichloromethane (40 mL), nitromethane (4 mL), $FeCl_3$ (0.70 g, 0.42 mmol). Silica gel column chromatography (dichloromethane/petroleum ether=1 : 1 v/v) and recrystallization with ethanol and ethyl acetate to obtain **LTP5** as a white solid (0.095 g, 93.8 %). ^{1}H NMR ($CDCl_3$, TMS, 400 MHz) δ (ppm): 9.00 (s, 2H, ArH), 8.52 (s, 2H, ArH), 8.29 (s, 2H, ArH), 8.11 (s, 2H, ArH), 7.87 (s, 4H, ArH), 4.39 (t, *J*=5.6 Hz, 4H, OCH_2), 4.29 (t, *J*=3.6 Hz, 12H, OCH_2), 1.97–2.07 (m, 16H, CH_2), 1.84 (s, 6H, $2CH_3$), 1.49–1.62 (m, 32H, CH_2), 1.00 (t, *J*=1.6 Hz, 24H, CH_3). ^{13}C NMR ($CDCl_3$, TMS, 100 MHz) δ (ppm): 152.28, 152.20, 149.75, 149.61, 148.93, 137.75, 137.69, 137.62, 128.75, 124.17, 116.53, 113.98, 108.56, 107.59, 107.36, 106.98, 106.84, 70.22, 69.64, 69.43, 46.82, 29.32, 29.21, 29.17, 28.79, 28.43, 28.41, 22.64, 22.63, 22.61, 14.16, 14.14. HRMS m/z (100 %) (MALDI): $[M]^+$ calcd for $C_{79}H_{106}O_8$ 1182.7888; Found 1182.7888. Elemental analysis: Calcd. for $C_{79}H_{106}O_8$: C 80.16 %, H 9.03 %. Found: C 79.80 %, H 8.70 %.

(**LTP8**) 2,3,6,7,12,13,16,17-Octakis(octyloxy)-20,20-dimethyl-20*H*-cyclopenta[1,2-*b* : 3,4-*b*']ditriphenylene. As above. **4 f** (0.20 g, 0.13 mmol), dichloromethane (60 mL), nitromethane (5 mL), $FeCl_3$ (0.11 g, 0.66 mmol). Silica gel column (dichloromethane/petroleum ether=1 : 2 v/v) and recrystallization with ethanol and ethyl acetate gave **LTP8** as a white solid (0.16 g, 80.4 %). ^{1}H NMR ($CDCl_3$, TMS, 400 MHz) δ (ppm): 9.00 (s, 2H, ArH), 8.52 (s, 2H, ArH), 8.30 (s, 2H, ArH), 8.12 (s, 2H, ArH), 7.88 (s, 4H, ArH), 4.32 (t, *J*=6.4 Hz, 16H, OCH_2), 1.94–2.04 (m, 16H, CH_2), 1.84 (s, 6H, $2CH_3$), 1.33–1.66 (m, 80H, CH_2), 0.91 (t, *J*=8 Hz, 24H, CH_3). ^{13}C NMR ($CDCl_3$, TMS, 100 MHz) δ (ppm): 152.25, 149.68, 149.56, 149.04, 148.96, 137.63, 128.88, 128.69, 124.41, 124.19, 116.54, 113.99, 108.58, 107.72, 107.22, 106.96, 70.23, 69.76, 69.67, 69.51, 46.78, 31.92, 31.88, 29.68, 29.59, 29.56, 29.54, 29.53, 29.52, 29.37, 28.75, 26.26, 26.24, 22.71, 14.12. HRMS m/z (100 %) (MALDI): $[M]^+$ calcd for $C_{103}H_{154}O_8$ 1520.1677; Found 1520.1668. Elemental analysis: Calcd. for $C_{103}H_{154}O_8$: C 81.37 %, H 10.21 %. Found: C 80.96 %, H 10.18 %.

(**LTP10**) 2,3,6,7,12,13,16,17-Octakis(decyloxy)-20,20-dimethyl-20*H*-cyclopenta[1,2-*b* : 3,4-*b*']ditriphenylene. As above. **4 g** (0.22 g, 0.13 mmol), $FeCl_3$ (0.10 g, 0.63 mmol) in chloroform (60 mL) and nitromethane (5 mL). Silica gel column chromatography (dichloromethane/petroleum ether=1 : 2 v/v). Recrystallization from ethyl acetate and ethanol gave a white solid **LTP10** (0.19 g, 88 %). ^{1}H NMR ($CDCl_3$, TMS, 400 MHz) δ (ppm): 9.00 (s, 2H, ArH), 8.52 (s, 2H, ArH), 8.30 (s, 2H, ArH), 8.12 (s, 2H, ArH), 7.88 (s, 4H, ArH), 4.27–4.40 (m, 16H, OCH_2), 1.95–2.06 (m, 16H, CH_2), 1.83 (s, 6H, CH_3), 1.60–1.68 (m, 16H, CH_2), 1.30–1.55 (m, 96H, CH_2), 0.88 (t, *J*=5.6 Hz, 24H, CH_3). ^{13}C NMR ($CDCl_3$, TMS, 100 MHz) δ (ppm): 152.11, 149.58, 149.41, 148.96, 148.81, 137.60, 128.82, 128.66, 124.34, 124.24, 124.08, 116.49, 113.94, 108.39, 107.39, 107.09, 106.63, 70.15, 69.63, 69.36, 46.76, 31.99, 29.78, 29.70, 29.65, 29.63, 29.60, 29.55, 29.48, 29.46, 28.82, 26.30, 22.76, 14.18, 14.16. HRMS m/s (MALDI): $[M]^{+\cdot}$ Calcd. for

$C_{119}H_{186}O_8$: 1744.4181; Found: 1744.4180. Elemental analysis: Calcd. for $C_{119}H_{186}O_8$: C 81.92 %, H 10.75 %; Found: C 81.94 %, H 10.51 %.

(**LTP12**) 2,3,6,7,12,13,16,17-Octakis(dodecyloxy)-20,20-dimethyl-20*H*-cyclopenta[1,2-*b* : 3,4-*b*']ditriphenylene. As above. **4 h** (0.18 g, 0.09 mmol), $FeCl_3$ (0.07 g, 0.46 mmol) in chloroform (60 mL) and nitromethane (5 mL). Silica gel column chromatography (dichloromethane/petroleum ether=1 : 2 v/v). Recrystallization from ethyl acetate and ethanol gave a white solid **LTP12** (0.12 g, 66 %). ^{1}H NMR ($CDCl_3$, TMS, 400 MHz) δ (ppm): 9.00 (s, 2H, ArH), 8.52 (s, 2H, ArH), 8.29 (s, 2H, ArH), 8.12 (s, 2H, ArH), 7.87 (s, 4H, ArH), 4.28–4.40 (m, 16H, OCH_2), 1.93–2.05 (m, 16H, CH_2), 1.83 (s, 6H, CH_3), 1.25–1.64 (m, 144H, CH_2), 0.86 (t, J=6.4 Hz, 24H, CH_3). ^{13}C NMR ($CDCl_3$, TMS, 100 MHz) δ (ppm): 149.62, 147.05, 146.90, 146.41, 146.30, 135.05, 126.28, 126.10, 121.79, 121.73, 121.54, 113.96, 111.40, 105.85, 104.95, 104.52, 104.19, 67.59, 67.09, 67.05, 66.86, 44.20, 29.40, 27.25, 27.22, 27.20, 27.16, 27.13, 27.06, 27.04, 27.01, 26.95, 26.86, 26.21, 23.73, 23.71, 20.17, 11.60, 11.58. HRMS m/s (MALDI): $[M]^{+\cdot}$ Calcd. for $C_{135}H_{218}O_8$: 1968.6685; Found: 1968.6686. Elemental analysis: Calcd. for $C_{135}H_{218}O_8$: C 82.34 %, H 11.16 %; Found: C 82.43 %, H 11.30 %.

(**LTP58**) 2,3,6,7,12,13,16,17-Octakis(pentyloxy)-20,20-dioctyl-20*H*-cyclopenta[1,2-*b* : 3,4-*b*']ditriphenylene. As above. **4 i** (0.18 g, 0.13 mmol), dichloromethane (50 mL), nitromethane (5 mL), $FeCl_3$ (0.11 g, 0.65 mmol). Silica gel column (dichloromethane/petroleum ether=1 : 1.5 v/v) and recrystallization with ethanol and ethyl acetate gave **LTP58** as a white solid (0.14 g, 80.0 %). ^{1}H NMR ($CDCl_3$, TMS, 400 MHz) δ (ppm): 9.00 (s, 2H, ArH), 8.41 (s, 2H, ArH), 8.30 (s, 2H, ArH), 8.12 (s, 2H, ArH), 7.89 (s, 4H, ArH), 4.31 (t, *J*=6.8 Hz, 16H, OCH_2), 2.28 (t, *J*=7.2 Hz, 4H, $2CH_2$), 1.94–2.05 (m, 16H, CH_2), 1.48–1.62 (m, 40H, CH_2), 1.01–1.08 (m, 16H, CH_2), 0.99 (t, *J*=1.2 Hz, 24H, CH_3), 0.70 (t, *J*=2.8 Hz, 6H, CH_3). ^{13}C NMR ($CDCl_3$, TMS, 100 MHz) δ (ppm): 149.69, 149.64, 149.39, 149.08, 149.04, 139.66, 128.87, 128.58, 124.47, 124.35, 124.26, 116.59, 113.69, 108.42, 108.03, 107.40, 107.09, 70.12, 70.10, 69.85, 69.75, 69.57, 55.10, 41.75, 31.74, 30.06, 29.56, 29.50, 29.25, 29.21, 29.20, 29.16, 29.12, 28.42, 28.40, 28.38, 28.37, 25.92, 25.89, 23.98, 22.70, 22.65, 22.63, 22.59, 22.57, 22.48, 14.15, 14.12, 14.08, 13.96. HRMS m/z (100 %) (MALDI): $[M]^+$ calcd for $C_{93}H_{134}O_8$ 1380.0112; Found 1380.0090. Elemental analysis: Calcd. for $C_{93}H_{134}O_8$: C 80.94 %, H 9.79 %. Found: C 80.58 %, H 9.86 %.

(**LTP88**) 2,3,6,7,12,13,16,17-Octakis(octyloxy)-20,20-dioctyl-20*H*-cyclopenta[1,2-*b* : 3,4-*b*']ditriphenylene. As above. **4 j** (0.25 g, 0.15 mmol), dichloromethane (70 mL), nitromethane (5 mL), $FeCl_3$ (0.12 g, 0.73 mmol). Silica gel column (dichloromethane/petroleum ether=1 : 2 v/v) and recrystallization from ethanol and ethyl acetate gave **LTP88** as a white solid. (0.18 g, 73.1 %). ^{1}H NMR ($CDCl_3$, TMS, 400 MHz) δ (ppm): 9.00 (s, 2H, ArH), 8.41 (s, 2H, ArH), 8.31 (s, 2H, ArH), 8.12 (s, 2H, ArH), 7.89 (s, 4H, ArH), 4.31 (t, *J*=1.2 Hz, 16H, OCH_2), 2.28 (t, *J*=1.2 Hz, 4H, $2CH_2$), 1.93–2.05 (m, 16H, CH_2), 1.00–1.63 (m, 104H, CH_2), 0.91 (t, *J*=2 Hz, 24H, CH_3), 0.70 (t, *J*=7.2 Hz, 6H, CH_3). ^{13}C NMR ($CDCl_3$, TMS, 100 MHz) δ (ppm): 149.65, 149.62, 149.39, 149.10, 149.05, 139.66, 128.87, 128.58, 124.47, 124.36, 124.30, 124.27, 116.59, 113.70, 108.37, 108.08, 107.46, 107.15, 70.09, 69.91, 69.79, 69.62, 55.11, 41.76, 31.91, 31.87, 31.75, 30.06, 29.61, 29.58, 29.56, 29.52, 29.49, 29.47, 29.38, 29.35, 29.22, 29.16, 26.27, 26.24, 26.21, 23.98, 22.70, 22.48, 14.13, 14.11, 13.96. HRMS m/z (100 %) (MALDI): $[M]^+$ calcd for $C_{117}H_{182}O_8$ 1716.3868; Found 1716.3863. Elemental analysis: Calcd. for $C_{117}H_{182}O_8$: C 81.86 %, H 10.69 %. Found: C 81.48 %, H 10.74 %.

(**LTP108**) 2,3,6,7,12,13,16,17-Octakis(decyloxy)-20,20-dioctyl-20*H*-cyclopenta[1,2-*b* : 3,4-*b*']ditriphenylene. As above. **4 k** (0.2 g, 0.10 mmol), dichloromethane (50 mL), nitromethane (5 mL), $FeCl_3$ (0.08 g, 0.51 mmol). Silica gel column (dichloromethane/petroleum ether=1 : 1.5 v/v) and recrystallization with ethanol and ethyl acetate gave **L108** (0.12 g, 60.1 %) as a white solid. ^{1}H NMR ($CDCl_3$, TMS, 400 MHz) δ (ppm): 8.99 (s, 2H, ArH), 8.41 (s, 2H, ArH), 8.31 (s, 2H, ArH), 8.12 (s, 2H, ArH), 7.90 (s, 4H, ArH), 4.31 (t, *J*=0.8 Hz, 16H, OCH_2), 2.28 (t, *J*=0.4 Hz, 4H, $2CH_2$), 1.93–2.05 (m, 16H, CH_2),

1.53–1.67 (m, 24H, CH_2), 1.00–1.45 (m, 112H, CH_2), 0.89 (t, *J*=6.8 Hz, 24H, CH_3), 0.70 (t, *J*=7.2 Hz, 6H, CH_3). ^{13}C NMR ($CDCl_3$, TMS, 100 MHz) δ (ppm): 149.65, 149.62, 149.39, 149.10, 149.05, 139.66, 128.87, 128.58, 124.47, 124.36, 124.30, 124.27, 116.59, 113.70, 108.37, 108.08, 107.46, 107.15, 70.09, 69.91, 69.79, 69.62, 55.11, 41.76, 31.91, 31.87, 31.75, 30.06, 29.61, 29.58, 29.56, 29.52, 29.49, 29.47, 29.38, 29.35, 29.22, 29.16, 26.27, 26.24, 26.21, 23.98, 22.70, 22.48, 14.13, 14.11, 13.96. HRMS m/z (100 %) (MALDI): $[M]^+$ calcd for $C_{133}H_{214}O_8$ 1940.6372; Found 1940.6363. Elemental analysis: Calcd. for $C_{133}H_{214}O_8$: C 82.29 %, H 11.11 %. Found: C 81.98 %, H 10.90 %.

Keywords: Columnar mesophases · Fluorescence · Gels · Organic semiconductors · Polyfused aromatic hydrocarbon (PAH)

Author Information

[a] J.-F. Hang, H. Lin, Prof. K.-Q. Zhao, Prof. P. Hu, Prof. B.-Q. Wang, College of Chemistry and Materials Science, Sichuan Normal University, Chengdu 610066, China, E-mail: kqzhao@sicnu.edu.cn

[b] Dr. H. Monobe, Nanomaterials Research Institute, National Institute of Advanced Industrial Science and Technology (AIST), Ikeda, Osaka, 5638577, Japan, E-mail: monobe-hirosato@aist.go.jp

[c] Dr. C. Zhu, Department Advanced Light Source, Lawrence Berkeley National Laboratory, 1 Cyclotron Rd., M/S 15R0217, Berkeley, CA 94720, USA

[d] Dr. B. Donnio, Institut de Physique et Chimie des Materiaux de Strasbourg (IPCMS), CNRS-Universite de Strasbourg (UMR 7504), Strasbourg, 67034, France, E-mail: bertrand.donnio@ipcms.unistra.fr

Acknowledgement

This research was financially supported by the National Natural Science Foundation of China (NSFC, Fund numbers: 51273133, 51773140, 51973143). KQZ and HM thank the support of NSFC-JSPS joint project (50811140156). BD thanks CNRS and University of Strasbourg for support.

Part of the joint “ECPM Strasbourg Institute Feature” Collection with EurJOC.

Conflict of Interest

The authors declare no conflict of interest.

Supporting information

Supporting information for this article is available on the WWW under https://doi.org/10.1002/ejoc.202100108

Biographical Information

Jun-Fang Hang was born in 1995 at Yunnan, China. He got his Bachelor Degree of Science in 2018 from Qujing Normal University. Now he is a Master degree student in Professor Ke-Qing Zhao group, with research work on synthesis and characterization of novel discotic liquid crystalline materials.

Hang Lin was born in Chengdu, China (1993). He received his BSc degree in Chemistry from Leshan Normal University (2017). Now he is a master's degree at Sichuan Normal University in Professor Ke-Qing Zhao group. He has won national scholarships, provincial first-prize scholarships for master's students, etc. His research interests focus on the design, synthesis and application of organic photoelectric functional materials and biomedical materials.

Dr. Ke-Qing Zhao is a professor of organic chemistry at Sichuan Normal University, Chengdu, China. He got his PhD from Sichuan University (1997) with Professor Liang-Fu Zhang as his supervisor, and went for a first postdoc fellowship at TU Darmstadt, Germany (2001–2002) in late Prof. Wolfgang Haase group, and a second one at the National Institute of Advanced Industrial Science and Technology (AIST), Japan (2002–2003) with Dr. Yo Shimizu as his collaborator. Recently he was a visiting scholar at Lawrence Berkeley National Lab, California USA (2019) in collaboration with Dr. Chenhui Zhu. Dr. Zhao has been doing research work in the field of molecular designing, synthesis and physical property studies of liquid crystalline semiconductors, with close collaboration with Dr. Bertrand Donnio (Strasbourg) and Dr. Hirosato Monobe (AIST).

Prof. Ping Hu is a Professor of Sichuan Normal University, Chengdu, China. Mr. Hu was born in 1964 at Sichuan, and graduated from Sichuan Normal University in 1985. His research interests include click chemistry to synthesis mesomorphic materials, metal organic liquid crystals, ionic liquid crystalline polymers, drugs and intermediates.

Prof. Bi-Qin Wang received her BSc from Sichuan Normal University in 1986 and has been working in the university since then. She worked as a visiting scholar at the Shanghai Institute of Organic Chemistry, Chinese Academy of Sciences in 1999, and at Peking University in 2007. She is now a full professor at Sichuan Normal University. Her current research interests focus on the development of new organic synthetic methods and the synthesis and property studies of organic functional materials.

Dr. Hirosato Monobe was born in Osaka, Japan. He obtained his Ph.D. in 1998 from Tokyo Institute of Technology, Yokohama under supervision of Prof. Masamichi Fujihira. In 1998 he was a fixed-term researcher at Osaka National Research Institute (merged with National Institute of Advanced Industrial Science and Technology, AIST in 2001). Then he was a researcher at AIST in 2001 and has been a senior researcher since 2005. He received the Encouragement Prize of the Japanese Liquid Crystal Society (2003) and the Young Scientist Award for the Presentation of an Excellent Paper of the Japan Society of Applied Physics (2004). His research interests focused on optical and electronic properties of liquid crystals for printed electronics and soft actuators.

Dr. Chenhui Zhu is a staff scientist at the Advanced Light Source in the Lawrence Berkeley National Laboratory, USA. He received his Ph.D in Physics from the University of Colorado in Boulder before he did his postdoctoral research at Argonne National Laboratory in Chicago. His research interests focus on the development of X-ray scattering tools such as resonant x-ray scattering and coherent scattering and their applications in materials science, including liquid crystals, polymers, metal organic frameworks, perovskite solar cells.

Dr. Bertrand Donnio completed his PhD on metal-containing liquid crystals at Sheffield University (UK) in 1996 (Pr. D. W. Bruce) and obtained his habilitation (HDR) from Strasbourg University in 2009. After two consecutive research fellowships with Pr. R. Deschenaux (Institut de Chimie, Neuchâtel, CH) and Pr. H. Finkelmann (Institüt für Makromolekulare Chemie, Freiburg, D), studying organometallic mesogens and then liquid crystalline elastomers, he was offered a research position at the CNRS in 1999. Promoted Director of Research in 2010, he spent a three-year sabbatical at UMI COMPASS (CNRS-SOLVAY-UPENN, Philadelphia, USA, 2013–2015). His current research interests focus on the synthesis of various supramolecular systems (liquid crystals, dendrimers, metal complexes), the investigation of mesomorphic organizations (S/WAXS), and the functionalization and precise self-assembly of metallic nanoparticles in periodic lattices.

References

[1] A. C. Grimsdale, K. L. Chan, R. E. Martin, P. G. Jokisz, A. B. Holmes, *Chem. Rev.* 2009, *109*, 897–1091.
[2] J. Li, A. C. Grimsdale, *Chem. Soc. Rev.* 2010, *39*, 2399–2410.
[3] C. Wang, H. Dong, W. Hu, Y. Liu, D. Zhu, *Chem. Rev.* 2012, *112*, 2208–2267.

[4] a) S. Sergeyev, W. Pisula, Y. H. Geerts, *Chem. Soc. Rev.* 2007, *36*, 1902–1929; b) T. Wohrle, I. Wurzbach, J. Kirres, A. Kostidou, N. Kapernaum, J. Litterscheidt, J. C. Haenle, P. Staffeld, A. Baro, F. Giesselmann, S. Laschat, *Chem. Rev.* 2016, *116*, 1139–1241; c) B. R. Kaafarani, *Chem. Mater.* 2011, *23*, 378–396.
[5] G. Hu, S. P. Kitney, M. R. Billa, S. M. Kelly, B. Lambert, W. Harrison, *Liq. Cryst.* 2021, *48*, 63–74.
[6] a) G. Hu, S. P. Kitney, S. M. Kelly, W. Harrison, M. O. Neill, *Liq. Cryst.* 2017, *44*, 1632–1645; b) G. Hu, M. R. Billa, S. P. Kitney, S. M. Kelly, *Liq. Cryst.* 2018, *45*, 965–979.
[7] M. Manickam, M. Belloni, S. Kumar, S. K. Varshney, D. S. Shankar Rao, P. R. Ashton, J. A. Preece, N. Spencer, *J. Mater. Chem.* 2001, *11*, 2790–2800.
[8] M. J. Sienkowska, H. Monobe, P. Kaszynski, Y. Shimizu, *J. Mater. Chem.* 2007, *17*, 1392–1398.
[9] K. Q. Zhao, J. Q. Du, X. H. Long, M. Jing, B. Q. Wang, P. Hu, H. Monobe, B. Henrich, B. Donnio, *Dyes Pigm.* 2017, *143*, 252–260.
[10] T. Yasuda, T. Shimizu, F. Liu, G. Ungar, T. Kato, *J. Am. Chem. Soc.* 2011, *133*, 13437–13444.
[11] a) V. Iguarbe, J. Barbera, J. L. Serrano, *Liq. Cryst.* 2020, *47*, 301–308; b) A. Concellon, R. Termine, A. Golemme, P. Romero, M. Marcos, J. L. Serrano, *Org. Chem. Front.* 2020, *7*, 2008–2015.
[12] S. W. Kim, D. M. Lee, J. H. Kim, E. J. Choi, C. J. Yu, *Liq. Cryst.* 2019, *46*, 1136–1144.
[13] a) S. Thiery, B. Heinrich, B. Donnio, C. Poriel, F. Camerel, *J. Phys. Chem. C* 2015, *119*, 10564–10575; b) S. Thiery, B. Heinrich, B. Donnio, C. Poriel, F. Camerel, *J. Mater. Chem. C* 2014, *2*, 4265–4275.
[14] W. W. H. Wong, T. B. Singh, D. Vak, W. Pisula, C. Yan, X. Feng, E. L. Williams, K. L. Chan, Q. Mao, D. J. Jones, C. Q. Ma, K. Mullen, P. Bauerle, A. B. Holmes, *Adv. Funct. Mater.* 2010, *20*, 927–938.
[15] W. W. H. Wong, C. Q. Ma, W. Pisula, A. Mavrinskiy, X. Feng, H. Seyler, D. J. Jones, K. Mullen, P. Bauerle, A. B. Holmes, *Chem. Eur. J.* 2011, 17, 5549– 5560.
[16] Y. Yang, H. Wang, H. F. Wang, C. X. Liu, K. Q. Zhao, B. Q. Wang, P. Hu, H. Monobe, B. Heinrich, B. Donnio, *Cryst. Growth Des.* 2018, *18*, 4296–4305.
[17] F. Lincker, A. J. Attias, F. Mathevet, B. Heinrich, B. Donnio, J. L. Fave, P. Rannou, R. Demadrille, *Chem. Commun.* 2012, *48*, 3209–3211.
[18] F. Lincker, B. Heinrich, R. D. Bettignies, P. Rannou, J. Pecaut, B. Grevin, A. Pron, B. Donnio, R. Demadrille, *J. Mater. Chem.* 2011, *21*, 5238–5247.
[19] a) B. Gomez-Lor, B. Alonso, A. Omenat, J. L. Serrano, *Chem. Commun.* 2006, 5012–5014; b) E. M. Garcia-Frutos, U. K. Pandey, R. Termine, A. Omenat, J. Barbera, J. L. Serrano, A. Golemme, B. Gomez-Lor, *Angew. Chem.* 2011, *123*, 7537–7540; *Angew. Chem. Int. Ed.* 2011, *50*, 7399–7402; c) E. M. Garcia-Frutos, A. Omenat, J. Barbera, J. L. Serrano, B. Gomez-Lor, *J. Mater. Chem.* 2011, 21, 6831–6836.
[20] a) K. Q. Zhao, C. Chen, H. Monobe, P. Hu, B. Q. Wang, Y. Shimizu, *Chem. Commun.* 2011, *47*, 6290–6292; b) L. L. Li, P. Hu, B. Q. Wang, W. H. Yu, Y. Shimizu, K. Q. Zhao, *Liq. Cryst.* 2010, *37*, 499–506; c) H. L. Ni, H. Monobe, P. Hu, B. Q. Wang, Y. Shimizu, K. Q. Zhao, *Liq. Cryst.* 2013, *40*, 411–420.
[21] a) S. Gomez-Esteban, A. Benito-Hernandez, R. Termine, G. Hennrich, J. T. Ljpez Navarrete, M. Carmen Ruiz Delgado, A. Golemme, B. Gomez-Lor, *Chem. Eur. J.* 2018, *24*, 3576–3583; b) W. Zhang, W. H. Yu, C. Feng, S. K. Xiang, B. Q. Wang, K. Q. Zhao, H. L. Ni, P. Hu, *Liq. Cryst.* 2020, *47*, 1100–1110; c) H. T. Xu, X. Xia, W. H. Yu, C. Feng, S. K. Xiang, B. Q. Wang, K. Q. Zhao, H. L. Ni, P. Hu, *Liq. Cryst.* 2021, *48*, 111–120; d) P. Ruan, B. Xiao, H. L. Ni, P. Hu, B. Q. Wang, K. Q. Zhao, Q. D. Zeng, C. Wang, *Liq. Cryst.* 2014, *41*, 1152–1161; e) K. Isoda, T. Yasuda, T. Kato, *Chem. Asian J.* 2009, *4*, 1619–1625.
[22] N. Miyaura, A. Suzuki, *Chem. Rev.* 1995, *95*, 2457–2483.
[23] a) M. Grzybowski, K. Skonieczny, H. Butenschon, D. T. Gryko, *Angew. Chem.* 2013, *125*, 10084–10115; *Angew. Chem. Int. Ed.* 2013, *52*, 9900–9930; b) M. Grzybowski, B. Sadowski, H. Butenschon, D. T. Gryko, *Angew. Chem.* 2020, *132*, 3020–3050; *Angew. Chem. Int. Ed.* 2020, *59*, 2998–3027; c) Y. Yang, J. Lan, J. You, *Chem. Rev.* 2017, *117*, 8787–8863.
[24] T. Ma, H. F. Wang, K. Q. Zhao, B. Q. Wang, P. Hu, H. Monobe, B. Heinrich, B. Donnio, *ChemPlusChem* 2019, *84*, 1439–1448.
[25] T. Ma, Y. J. Zhong, H. F. Wang, K. Q. Zhao, B. Q. Wang, P. Hu, H. Monobe, B. Donnio, *Chem. Asian. J.* DOI: 10.1002/asia.202100173.
[26] a) K. C. Zhao, J. Q. Du, H. F. Wang, K. Q. Zhao, P. Hu, B. Q. Wang, H. Monobe, B. Heinrich, B. Donnio, *Chem. Asian J.* 2019, *14*, 462–470; b) C. X. Liu, H. Wang, J. Q. Du, K. Q. Zhao, P. Hu, B. Q. Wang, H. Monobe, B. Henrich, B. Donnio, *J. Mater. Chem. C.* 2018, *6*, 4471–4478.
[27] K. Q. Zhao, Y. Gao, W. H. Yu, P. Hu, B. Q. Wang, B. Heinrich, B. Donnio, *Eur. J. Org. Chem.* 2016, 2802–2814.
[28] H. Huang, Q. Fu, B. Pan, S. Zhuang, L. Wang, J. Chen, D. Ma, C. Yang, *Org. Lett.* 2012, *14*, 4786–4789.
[29] S. Kumar, Y. T. Tao, *J. Org. Chem.* 2015, *80*, 5066–5076.
[30] F. Morale, R. W. Date, D. Guillon, D. W. Bruce, R. L. Finn, C. Wilson, A. J. Blake, M. Schroder, B. Donnio, *Chem. Eur. J.* 2003, *9*, 2484–2501.

[31] B. Donnio, B. Heinrich, H. Allouchi, J. Kain, S. Diele, D. Guillon, D. W. Bruce, *J. Am. Chem. Soc.* 2004, *126*, 15258–15268.
[32] D. Myśliwiec, B. Donnio, P. J. Chmielewski, B. Heinrich, M. Stępień, *J. Am. Chem. Soc.* 2012, *134*, 4822–4833.
[33] S. S. Babu, V. K. Praveen, A. Ajayaghosh, *Chem. Rev.* 2014, *114*, 1973–2129.
[34] H. Monobe, Y. Shimizu, S. Okamoto, H. Enomoto, *Mol. Cryst. Liq. Cryst.* 2007, *476*, 31–41.
[35] D. Adam, P. Schuhmacher, J. Simmerer, L. Haussling, K. Siemensmeyer, K. H. Etzbachi, H. Ringsdorf, D. Haarer, *Nature* 1994, *371*, 141–143.
[36] R. J. Bushby, S. M. Kelly, M. O'Neill, in *Liquid crystalline semiconductors. Materials, properties and applications.* Springer Series in Materials Science, Springer, Dordrecht, 2013, vol. 169.